AAAS
Research
Volume 2019, Article ID 2581241, 10 pages
https://doi.org/10.34133/2019/2581241

Research
OFFICIAL JOURNAL OF CAST

Research Article

How Pore Hydrophilicity Influences Water Permeability?

Fang Xu, Mingjie Wei, Xin Zhang, Yang Song, Wei Zhou, and Yong Wang*

State Key Laboratory of Materials-Oriented Chemical Engineering, Jiangsu National Synergetic Innovation Center for Advanced Materials, and College of Chemical Engineering, Nanjing Tech University, Nanjing 211816, Jiangsu, China

*Correspondence should be addressed to Yong Wang; yongwang@njtech.edu.cn

Received 2 November 2018; Accepted 10 January 2019; Published 4 February 2019

Copyright © 2019 Fang Xu et al. Exclusive Licensee Science and Technology Review Publishing House. Distributed under a Creative Commons Attribution License (CC BY 4.0).

Membrane separation is playing increasingly important role in providing clean water. Simulations predict that membrane pores with strong hydrophobicity produce ultrahigh water permeability as a result of low friction. However, experiments demonstrate that hydrophilic pores favor higher permeability. Herein we simulate water molecules transporting through interlayers of two-dimensional nanosheets with various hydrophilicities using nonequilibrium molecular dynamics. We reveal that there is a threshold pressure drop (ΔP_T), exceeding which stable water permeability appears. Strongly hydrophobic pores exhibit extremely high ΔP_T, prohibiting the achievement of ultrahigh water permeability under the experimentally accessible pressures. Under pressures < ΔP_T, water flows in hydrophobic pores in a running-stop mode because of alternative wetting and nonwetting, thus leading to significantly reduced permeability. We discover that hydrophilic modification to one surface of the nanosheet can remarkably reduce ΔP_T by > 99%, indicating a promising strategy to experimentally realize ultrafast membranes.

1. Introduction

Membrane separation is playing a key role in supplying potable water to people's daily life and industry [1]. Separation performances are significantly influenced by the hydrophilicity of the membrane pores. However, there are contradictory observations between experimental and simulation studies in the influence of membrane hydrophilicity on water permeability. Experimentally, it is commonly acknowledged that membranes for applications ranging from microfiltration to reverse osmosis (RO) should have strong hydrophilicity to ensure adequate water permeabilities [2–4]. Oppositely, molecular dynamics (MD) simulations demonstrate that hydrophobic pores favor enhanced water flux [5–8]. When water is confined in subnanometer pores, *e.g.,* in nanofiltration (NF) or RO membranes [9], there would be only one or two water layers inside the pores; *i.e.,* all the water molecules are included in the boundary layer. Therefore, the interaction between water molecules and pore walls would significantly influence water transport. Hydrophilicity increases the interaction between water molecules and pore walls and influences water permeability of a membrane from two opposite sides. On one hand, the positive side, the hydrophilic interaction could increase the infiltration capillary force, helping the membrane to uptake water molecules and to increase the membrane wettability. The infiltration capillary force increases dramatically with decreasing pore sizes. When the pore size is narrowed down to the subnanometer scale, water molecules inside the membrane will have greater probability to form hydrogen bonded networks, which plays an important role for water transport in the confined environment [10]. On the other hand, the negative side, stronger interaction between water molecules and pore walls results in increased friction and consequently reduces the flow velocity [11]. Larger proportion of water molecules will interact with the pore wall as the pore size decreases, and thus the friction effect becomes more pronounced. Therefore, it is necessary and worthwhile to investigate the combination effect of these two sides on water permeability.

Specifically, the recently emerging laminated membranes established from two-dimensional (2D) materials have subnanometer interlayer gaps, which offer slit-shaped pores for water transport [12–17]. In studies of these membranes, there also exists contradiction between experimental observations and simulation results on how the pore hydrophilicity influences the permeability. In experiments, Sun *et al.* [17] reported a laminar MoS_2 membrane exhibiting a 3- to 5-times higher water flux than the graphene oxide (GO) membrane. They attributed the improved flux to the exposure of the hydrophilic sulfur atoms in the MoS_2 monolayer

sheets. Ren *et al.* [18] fabricated ion separation membranes from nanosheets of $Ti_3C_2T_x$ MXene and they believed the promoted water flow was due to the hydrophilic nature of $Ti_3C_2T_x$. In contrast, by MD simulations, Wei *et al.* [19] found that the flow rate exhibited a significant enhancement between graphene layers, but the enhancement broke down while the graphene sheets were modified with hydrophilic groups. Moreover, Chen *et al.* [20] simulated water transport through GO interlayers with various concentrations of hydrophilic hydroxyl groups and found that the volumetric flux was negatively related to hydroxyl concentrations, implying that stronger hydrophilicity was unfavorable for water transport. This contradiction between experimental and simulation results confuses the understanding on the effect of pore hydrophilicity on water permeability. Therefore, identifying the origin of this contradiction is of great significance not only for deeper understanding on the role of material hydrophilicity in water transport but also for the design and preparation of ultrafast membranes.

In this work, we simulate water transport through pores constructed from 2D nanosheets with various hydrophilicities by using nonequilibrium molecular dynamics (NEMD). We reveal that strong hydrophobicity leads to high water permeability but also high threshold pressure drop (ΔP_T), and only the applied pressure drop exceeds ΔP_T; the high permeability can occur. For hydrophobic membranes, ΔP_T's are typically at the scale of several hundreds of MPa, far more than experimentally accessible pressure drops. This explains why we seldom experimentally observe simulation-predicted ultrahigh water permeability on hydrophobic membranes. Based on these understandings we develop a new strategy—hydrophilic modification to the outer pore surface—to efficiently reduce ΔP_T of hydrophobic membranes to the experimentally accessible scale at slight expense of permeability loss, thus enabling the experimental realization of ultrafast membranes.

2. Results

2.1. Apparent Flux and Permeability. We calculate the water flux of membranes with varying hydrophilicities under pressure drops (ΔPs) ranging from 100 to 600 MPa by fitting the slope of the flow curve (Figure S1). As shown in Figure 1(a), the flux of each membrane is proportional to ΔP despite the changing hydrophilicities. However, to achieve the continuous water flow ΔPs should be higher than a certain value, beyond which the proportional relationship between flux and ΔP is valid. For hydrophilic membranes (contact angles, CAs $< 95^\circ$), the proportional relationship is valid from 100 MPa. For the membrane with CA= 120°, no water flux can be produced under ΔPs < 200 MPa. For the most hydrophobic membrane (CA = 138°), ΔP should be raised to nearly 400 MPa to obtain the continuous water flow. Apparently, these ΔPs are much larger than those applied in experiments. Therefore, we denote the water flux or permeability under such high ΔPs as apparent flux or apparent permeability as they will hardly be obtained in experiments. Figure 1(b) presents the apparent permeabilities of each membrane, which are obtained by directly fitting the flux values in Figure 1(a). It is obvious that the hydrophilicity of membranes plays a key role in governing water permeability. The permeability increases monotonically with rising hydrophobicity. Other simulation works give similar results no matter how they tune the hydrophilicity of the membrane, such as scaling the *vdW* interactions strength [21], applying artificial surface partial charge patterns [5], adjusting the density of hydroxyl groups [20], or utilizing different substances [6]. That is, all simulation works demonstrate a negative correlation between water flux and hydrophilicity.

2.2. Water Transport in Hydrophobic Membranes. As mentioned above, for hydrophobic membranes (CAs > 120°), no water molecule could pass through the pores and consequently no flux was measured under the ΔP of 100 MPa. This implies that the proportional relationship between flux and ΔP cannot extend to the region of lower ΔPs. For the most hydrophobic membrane with a CA of 138°, the proportional relationship starts around 400 MPa. However, it does not necessarily imply that it gives no flux under ΔPs below 400 MPa. We further simulated its flux under lower ΔPs with smaller pressure intervals to reveal the relationship in a broader range of ΔPs. As shown in Figure 1(c), it is obvious that water flux of the hydrophobic membrane (CA = 138°) is not proportional to ΔP and instead there exists three stages within the range of ΔPs from 100 to 600 MPa. In the first stage where ΔP < 220 MPa, no evident water flux is observed. It is found that there is no water molecule inside the membrane, indicating the nonwetting state of the membrane. In the second stage, where ΔP ranges from 220 to 350 MPa, the water flux rises rapidly. In the last stage, the water flux is proportional to ΔPs. In contrast, for the hydrophilic membrane with a CA of 29° the water flux is always proportional to ΔP within the entire range of ΔP, implying that under high ΔPs hydrophobic pores exhibit a wetting state similar to hydrophilic pores.

To elucidate the three-staged relationship between water flux and ΔP for the membrane with the CA of 138°, we investigated the microscopic details of water molecules inside this hydrophobic membrane under different ΔPs. We recorded the number of water molecules in the permeate side as a function of simulation time, which is shown in Figure 1(d). Sufficient water molecules were provided to the feed side so that the simulation can continue for adequate time. The evolution of the number of permeated water molecules demonstrates that the flow rate of water through the membrane is constant under 400 MPa (in the third stage), which is also similar to water passing through the membrane with a CA of 29° shown in Figure S1. However, there appears many steps in the flow curve in the case of 250 MPa (in the second stage), which implies a discontinuous water flow. This is actually a running-stop mode including alternative "running" and "stop" states.

To quantitatively investigate this "running-stop" water flow, we monitored the number of water molecules inside the membrane (N_{water}) during the entire flow process and revealed the tendency of its variations. Figure 2(a) illustrates the probability distribution of N_{water} under four different ΔPs spanning from the second to the third stage. In the case

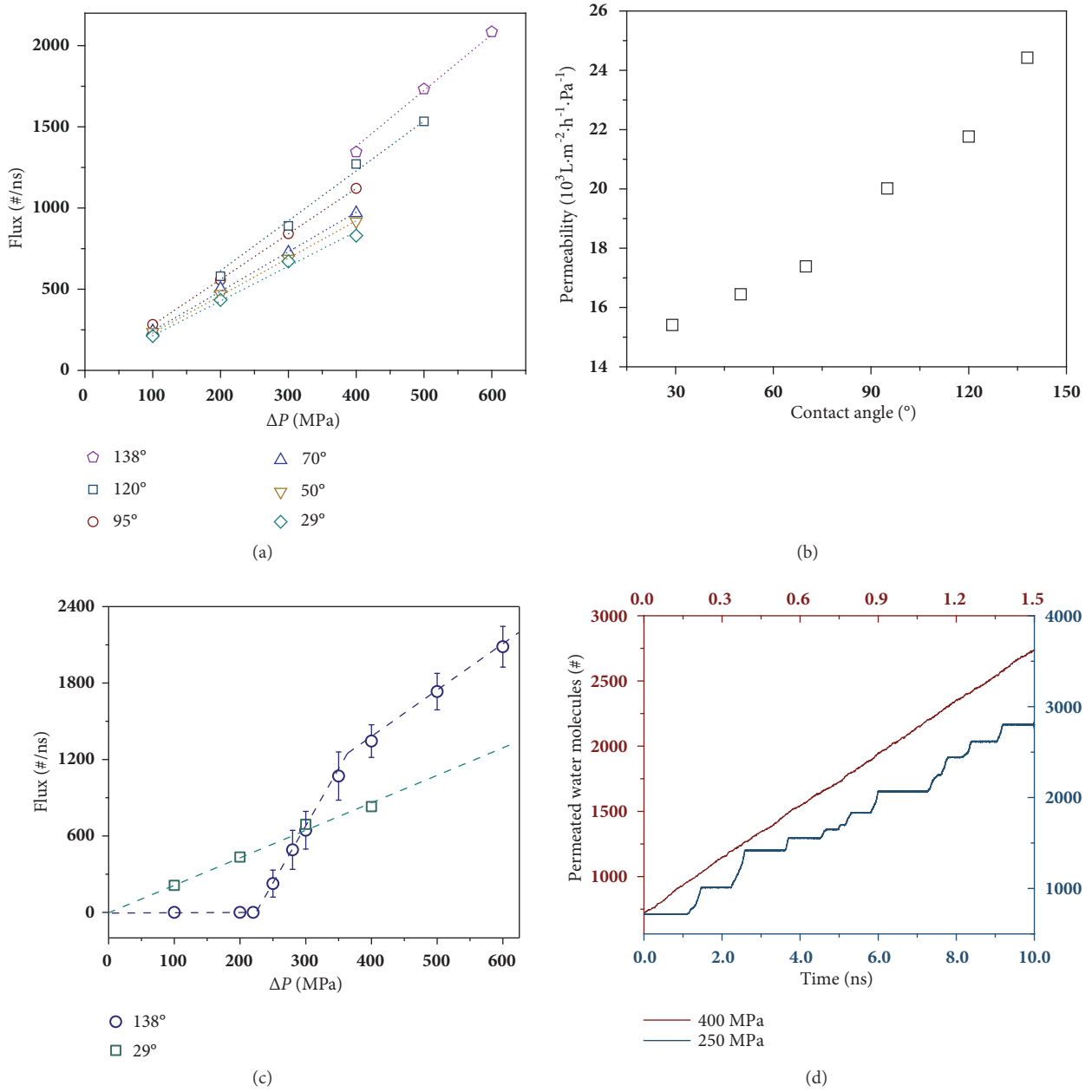


FIGURE 1: Flux and permeability. (a) Water flux and (b) permeability of membranes with various hydrophilicities represented by changing CAs. (c) Water flux of membranes with the CA of 29° and 138° within the ΔP range from 100 to 600 MPa. (d) Number of water molecules in the permeate side of the membrane with the CA of 138° under two typical ΔPs (250 and 400 MPa) as a function of simulation time.

of 400 MPa, N_{water} is distributing near 250, indicating that the number of water molecules remains ~250 during the simulation time. Nevertheless, when ΔP is decreased from 400 MPa to 250 MPa, N_{water} distributes in an increasingly wide range, indicating that the pores are not completely filled with water during the entire simulation time. As vividly shown in the snapshots in Figure 2(b), water streams inside the pores under these ΔPs break off during the flowing process. This results in water transport in the running-stop mode.

When the system reaches a steady state, the driving force and resistance are in balance, which leads to a continuous water flow and a stable flux. Oppositely, the running-stop transport is a metastable state with a wetting and a nonwetting state repeating alternately rather than a stable continuous flow. The hydrogen bonded network that stretched from the entrance to the exit of the pore was reported to be responsible for the fast transport in membranes made of 2D grapheme [12]. Moreover, the hydrogen bonded network must be reformed when water molecules enter highly confined pores [22, 23]. Based on these understandings, we realize that in the second stage the wetting behavior of water molecules cycles between the wetting state and the nonwetting state. In the wetting state, the hydrogen bonded

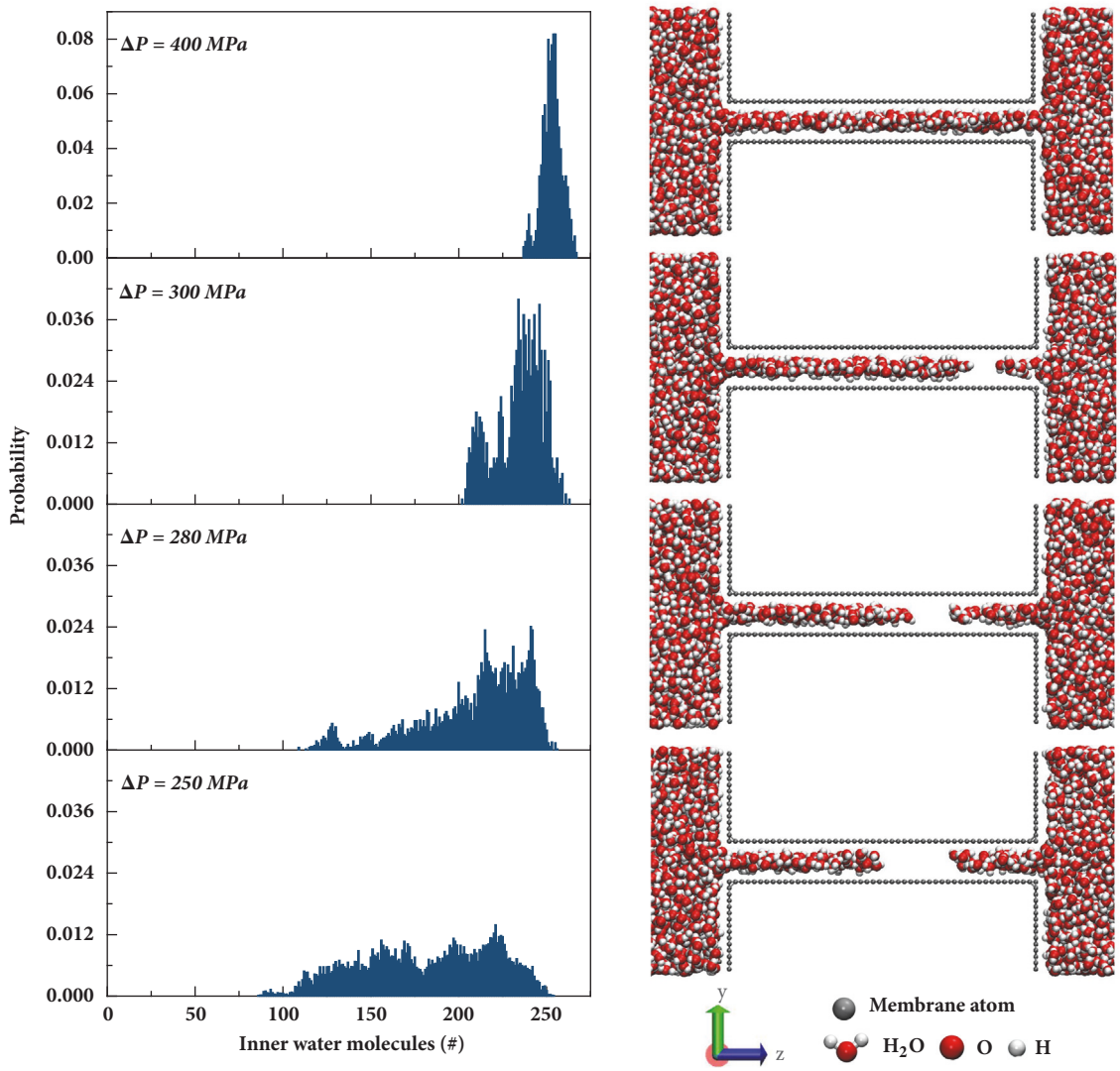


FIGURE 2: Wetting behavior of hydrophobic membranes under various ΔPs. (a) Probability of the number of water molecules inside the pores under different ΔPs. (b) Representative snapshots of the water stream inside the pore during the flowing process under the corresponding ΔP. The water molecules are presented in red (oxygen atom) and white (hydrogen atom). The membranes are colored in grey.

network completely forms, therefore, the running state is reached and the flow occurs. However, in the nonwetting state, the water stream is disconnected as the hydrogen bonded network breaks, terminating water flow (the stop state). Figure 2(a) shows N_{water} distributes in wider ranges with decreasing ΔPs, indicating the running state lasts shorter and the stop state last longer. Consequently, lower water permeabilities are obtained under decreasing ΔPs. When the ΔP is decreased to be lower than 220 MPa, the stop states (nonwetting) dominate, and consequently no flux can be observed. Similarly, the transport mode would turn into the constant running state (wetting) when the ΔP rises to a certain value, beyond which the water flux becomes always proportional to ΔPs.

2.3. The Threshold Pressure Drop. We term this critical ΔP, above which the pores are in the wetting state and water flow reaches the constant running state, the threshold pressure drop, ΔP_T. The ΔP_T's for membranes with various CAs are plotted in Figure 3. For hydrophilic membranes (CA = 29°, 50°, or 70°), the ΔP_T's are nearly zero because these hydrophilic membranes could be constantly wetted and no external pressure is needed. For hydrophobic membranes, the ΔP_T appears and rises rapidly with increasing CAs. Now we understand that higher hydrophobicity leads to greater water permeability but higher ΔP_T's. ΔPs used in experimental works generally exceed ΔP_T's of hydrophilic membranes, so one could easily obtain the continuous flux. For hydrophobic membranes, the ΔP_T's are much higher than experimental

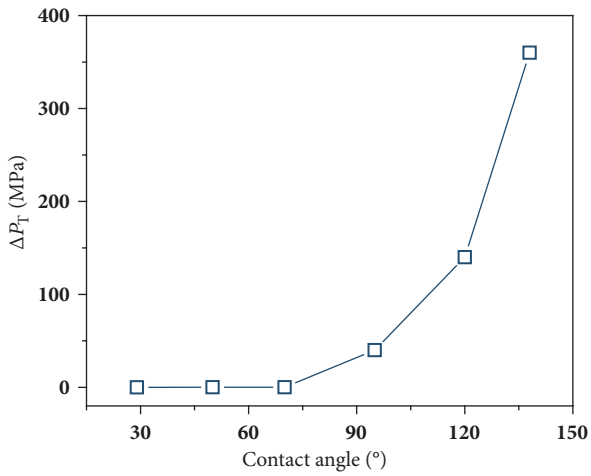


FIGURE 3: Threshold pressure drops (ΔP_T's) for membranes with various hydrophilicities indicated by CAs increased from 29° to 138°.

pressures, and it is difficult to wet the pores under the experimentally used ΔPs, resulting in no water permeability. In contrast, in simulations the employed ΔPs are typically in the scale of several hundreds of MPa, generally exceeding the ΔP_T's of both hydrophobic and hydrophilic membranes, and both membranes can reach the wetting state. Once wetted, hydrophobic membranes exhibit higher water permeabilities than hydrophilic ones due to the low friction of the former, as shown in Figure 1(b). This explains the contradictory results between experiments and simulations with respect to the influence of pore hydrophilicity on the water permeability.

2.4. Modification Strategies to Reduce Threshold Pressure Drop. Hydrophobic membranes exhibit ultrahigh water permeabilities, but only under extremely high pressures because of their high ΔP_T's. Therefore, to experimentally realize the ultrahigh permeabilities, the ΔP_T's of hydrophobic membranes should be significantly depressed to the scale close to the experimentally used ΔPs. ΔP_T's are dependent on the wetting state of the membrane. Therefore, suitably changing the wetting behavior of the membranes by hydrophilic modification may reduce ΔP_T's at no or little expense of water permeabilities. In addition to the complete hydrophilic modification to pore walls, which totally eliminates the pristine hydrophobicity of the pores and consequently the ultrahigh permeability, there has emerged a few other strategies to perform hydrophilic modification on selective positions of 2D nanosheets, that is, hydrophilic modification to the pore entrances [24] and regionally hydrophilic modification inside the pores [12, 25]. We then examine their efficiency in reducing ΔP_T's.

In the first strategy, the hydrophilic modification was applied only to the entrance region while the inner pore was still kept its pristine hydrophobicity (with CA of 95°, 120°, or 138°). The entrance region was defined as 5 Å from the inlet of the pore and modified with atoms to give a CA of 29°. We investigated the wetting behavior and the permeability under both low and high ΔPs. As shown in Figure 4(a), water molecules could occupy only the modified part at the entrance region under low ΔPs (≤1 MPa), suggesting that the ΔP_T exists not only at the entire entrance region, but throughout the inner hydrophobic area. As a result, we did not observe any water molecules passing through the membranes. Under high ΔPs (hundreds of MPa), the water flux also experience the three-staged flow as described above. Moreover, no evident change of ΔP_T for these membranes with various CAs is observed. The ΔP_T in this case is still as high as that for the unmodified hydrophobic membrane, indicating that this hydrophilic modification takes little effect on depressing the ΔP_T.

Hydrophilic modification to graphene is frequently achieved by oxidation [26], and the generated oxygen-containing groups prefer to form clusters, which resulting in the patches of pristine (hydrophobic) and oxidized (hydrophilic) regions on the surface of grapheme [27–29]. This can be considered as regionally hydrophilic modification inside the pore. To find out the influence of this modification on water permeability, the pore wall was patterned with two regions: one-half is hydrophilic (CA = 29°) and the other is hydrophobic (CA = 95°, 120°, or 138°). Under low ΔPs, there are two distinctive wetting states for membranes with different hydrophilicities. When the hydrophobicity is moderate (CA = 95°), water molecules start to occupy the hydrophilic region and then saturate the hydrophobic region progressively, indicating that the impact of hydrophilic interaction help to uptake more water molecules into the pores. Ban *et al.* [30] also observed that water first saturated the oxidized regions and then flooded to the pristine regions in GO membranes. ΔP_T of this modified membrane is significantly decreased from ~ 40 MPa for the pristine membrane to less than 0.1 MPa, while the permeability under high ΔPs is moderately decreased from ~20×10^3 to ~17×10^3 $L\cdot m^{-2}\cdot h^{-1}\cdot MPa^{-1}$.

However, as can be seen from Figure 4(b) when the CA of the hydrophobic region is higher than 120°, water molecules would not wet the hydrophobic region after covering the hydrophilic region. This implies that the ΔP_T of the hydrophobic region cannot be depressed by this regional modification. The nonwetting state of the hydrophobic regions in the pores means that the actual porosity under this condition turns into only half of the pristine one, thus, the flux will not be higher than half of the pristine one. While under high ΔPs, water molecules fill the membrane completely like that in the unmodified hydrophobic membrane, however the water permeability is lower compared to the unmodified hydrophobic membrane. Wei *et al.* [25] attributed this to a prominent side-pinning effect. Due to the inconsistence of wetting under low and high ΔPs, it is unreliable to extrapolate the permeability under high ΔPs to those under low ΔPs. Therefore, we understand that the regional hydrophilic modification cannot depress ΔP_T's of strongly hydrophobic membranes although it works for moderately hydrophobic membranes (CA < 120°).

Alternatively, we propose another strategy, that is, hydrophilic modification to the outer pore walls, which can efficiently reduce ΔP_T's of strongly hydrophobic membranes (CA = 120° or higher). The fast water transport through

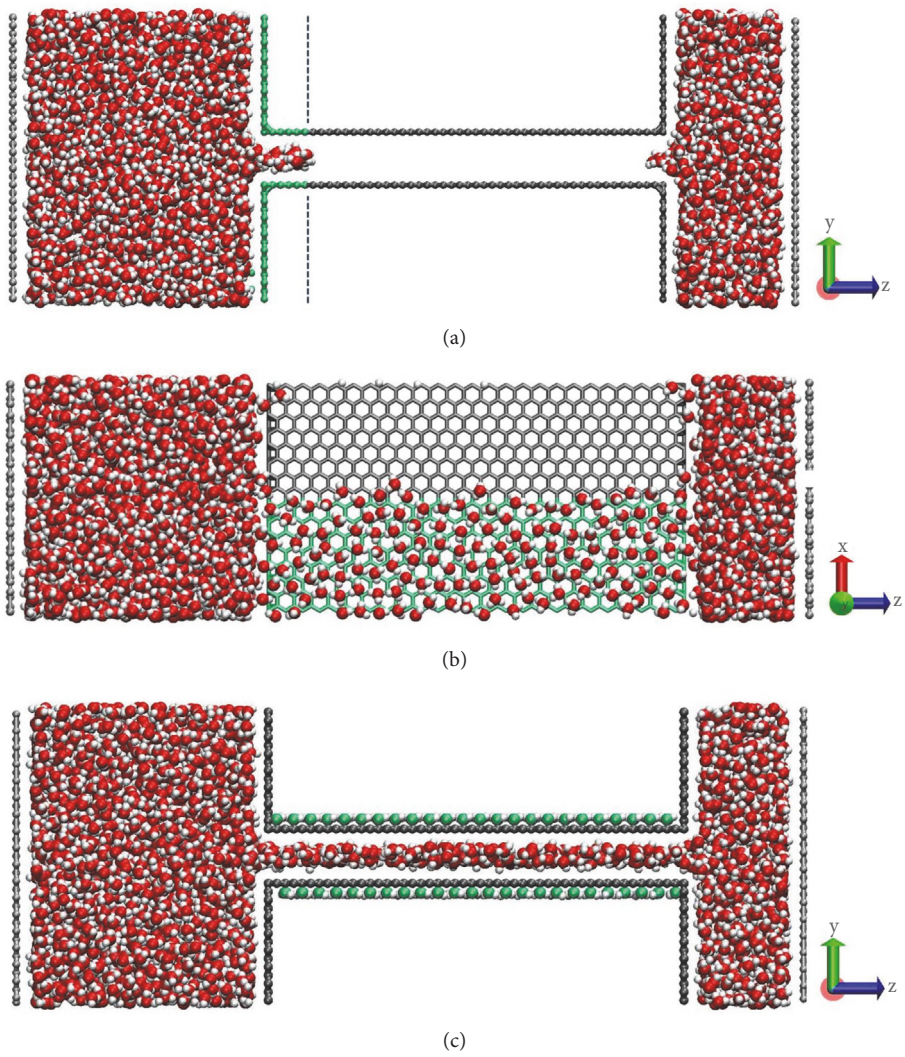


FIGURE 4: Three simulation models and the wetting states of hydrophobic membranes subjected to different hydrophilic modifications under ΔP =1 MPa. (a) Hydrophilic modification to the pore entrances; (b) regionally hydrophilic modification inside the pore; (c) hydrophilic modification to the outer pore walls. Green and dark grey represent the hydrophilic and hydrophobic part, respectively, and oxygen and hydrogen atoms in hydroxyl groups are marked in green and white, respectively.

graphene interlayers is prohibited by the hydrophilic oxygen-containing groups inside the pores [19, 20]. This is because the interaction between water and hydrophilic groups is too strong. Considering that 2D monolayer nanosheets are only one-atom thick, we anticipate that presence of these groups on the outer surface will reduce the interaction to some degree but will not fully eliminate it. Thus, the modification to the outer walls may also affect the water transport inside the pore across this one-atom thickness. As shown in Figure 4(c), the commonly used hydrophilic hydroxyl groups are chosen to functionalize the outer walls. The hydroxyl groups were randomly distributed outside the pore wall with concentration $c = n_{OH}/n_C$ = 24%, which is similar to both experimental [31, 32] and simulation [20] results. The all-atom optimized potential for liquid simulations (OPLS-AA) [33] was used for the functional groups, which is successfully applied in previous studies on the graphene oxides membrane [19, 25, 34].

We investigated the membrane with the CA of 120°, whose ΔP_T cannot be reduced by the strategy of regional modification as we discussed above. By hydrophilic modification to the outer surface the pore could be wetted under low pressures (~1 MPa), suggesting that the ΔP_T is depressed over 99% as it is ~140 MPa for the pristine membrane. Meanwhile, the permeability under high ΔPs, which is the slope of the flux-ΔP curve, is decreased by only 10 % (Figure 5(a)) and this value could be applied to the low ΔPs due to the consistence of their wetting states. Moreover, to exclude the particularity of the channel size, we also applied this method to 0.7 nm-wide pores, and obtain similar results as shown in Figure 5(b). Furthermore, Figure 5 also indicates that thus modified membranes exhibit much higher

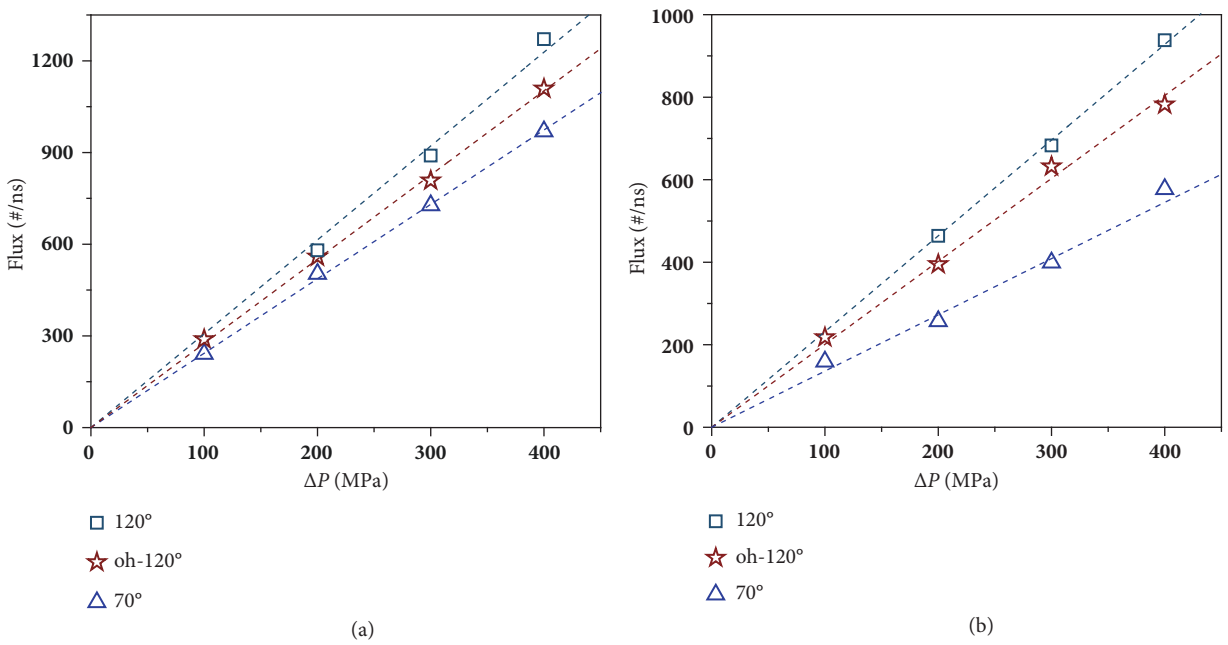


FIGURE 5: Flux of the (a) 0.8 nm-wide and (b) 0.7 nm-wide pores with different CAs. "oh-120°" indicates the membrane with a CA of 120° for the inner pore surface and the outer pore surface subjected to hydrophilic modification.

water permeability than initially hydrophilic membranes, for instance, the membrane with a CA of 70°. Therefore, we conclude that hydrophilic modification to the outer pore surface is a highly efficient strategy to reduce ΔP_T at slight expense of water permeability. This modification strategy requires hydrophilic modification exclusively on one side of 2D monolayers while keeps the strong hydrophobicity of the other side intact. Importantly, such a "Janus" 2D structure has already been experimentally obtained [35, 36], implying the big potential to experimentally realize ultrafast membranes by this hydrophilic modification strategy.

3. Discussion

In summary, membranes were constructed from 2D nanosheets with varying hydrophilicities to investigate the contradiction between experimental and simulation results on the influence of the pore hydrophilicity on water transport. We discover that the contradiction originates from the discrepancy of pressure drops (ΔP) in experiments and simulations. For hydrophilic membranes, there is a proportional relationship between flux and ΔPs. In contrast, for hydrophobic membranes, this proportional relationship only exits under high ΔPs. Under a threshold pressure drops, ΔP_T, there is no flux or a discontinuous water flow in the "running-stop" mode. In simulations, the ΔP is usually set to be extremely high to accelerate the computing. This high ΔP could facilely exceed the ΔP_T, so that the membranes are always in the wetting state. The different wetting states hinder the extrapolation of permeability from high ΔP's to low ΔP's, leading to the contradictory understanding on the effect of hydrophilicity. Unlike the hydrophobic membranes, the hydrophilic membranes could be wetted under low ΔPs, indicating ΔP_T is nearly zero. We investigate the efficiency of different hydrophilic modifications in depressing ΔP_T's of hydrophobic membranes and propose a new strategy, hydrophilic modification of the outer pore wall, which is able to depress ΔP_T's by > 99% of highly hydrophobic membranes at the slight expense of ~ 10% reduction in water permeability. This work identifies the origin of the contradictions between experimental and simulation results on the effect of pore hydrophilicity on water permeability, which not only helps to understand water transport in nanopores but also to design and experimental realization of ultrafast membranes.

4. Methods

The simulation system consisted of a membrane with one water reservoir and one additional moveable piston at each end, as shown in Figure S2. A 2D nanosheet bilayer was set to be parallel to the *yz* plane and modeled as the slit pore, and the length of the pore was set to 6 nm while the thickness of the pore was set to 0.8 nm, which was based on the interlayer spacing of the graphene oxide membrane [12, 31, 37]. Another four constraint walls (vertical to the pore wall and parallel to the *xy* plane) were served as the membrane surfaces, which were used to embed the pores and restrict the movement of water molecules. Such a membrane model is reliable and has also been adopted in other MD simulations [21]. The two water reservoirs formed the feed side (high pressure) and the permeate side (low pressure). Hence, the flow direction through the membrane was defined along the *z* direction. Besides, the system was bounded by two rigid pistons used to create a pressure drop (ΔP) across the membrane. The simulation box lengths in *x* and *y* directions are set equal to

the lateral size of the bilayer (34.3 Å) and the height of four constraint walls (43.7 Å), respectively.

All the simulations were carried out using the large-scale atomic/molecular massively parallel simulator (LAMMPS) package. The SPC/E model was utilized to construct the water molecules. The SHAKE algorithm was applied to constrain the bonds and angles of the water molecules, which reduced high frequency vibrations and saved the simulation time. The interaction for all atoms included *vdW* and electrostatic terms. The former was modeled with a LJ potential, $4\varepsilon[(\sigma/r)^{12}\text{-}(\sigma/r)^{6}]$, and the cutoff was set as 1.0 nm. In this work, the structure of graphene was merely used as the channel model. According to Werder *et al.* [38], the hydrophilicity of the membrane could be tuned by changing the ε parameter between C and O atoms while keeping the σ parameter fixed. The ε parameter signifies a microscopic interaction, which is not a macroscopic manifestation of hydrophilicity. In addition, the CA of a water droplet on a surface is usually employed to measure the membrane hydrophilicity, which is a macroscopic manifestation of the microscopic interactions between the surface and the water molecules. Hence, according to the work studying the CA of water on 2D planes with varying ε parameters [38], we also adopt the CAs ranging from 29° to 138° to characterize and distinguish the membranes with varying hydrophilicities. This method to adjust hydrophilicity was reported to have a negligible effect on the channel diameter [39]. The long-range electrostatic interactions are computed by using the particle-particle particle-mesh (PPPM) algorithm with a root mean square accuracy of 10^{-5}. The membrane models were fixed in position throughout the simulation, and periodic boundary conditions (PBC) were applied in the x and y directions. A time step of 1 fs was used for all simulations.

Initially, for each simulation, the energy of system was minimized for 1000 steps. Then an external force along the -z/+z direction, f, is applied to each atom of top/bottom piston to produce a pressure of 1 atm (Equation (1)), allowing the system to reach the desired pressure and the bulk water to reach the equilibrium density (1 g/cm^3).

$$f = \frac{PA}{n} \tag{1}$$

where P denoted the desired pressure on the piston, A was the area of the piston, and n represented the atom number of the piston. The system was kept at room temperature (300K) using the Berendsen thermostat. After the equilibrium simulation of 2 ns, the NEMD simulations were carried out by applying another external force on the bottom piston, so the ΔP could be calculated by

$$\Delta P = P_{bottom} - P_{top} \tag{2}$$

After the first 1 ns of stabilization of the NEMD simulation, statistics and trajectories were gathered during 2-10 ns for different systems, which was long enough to obtain the well-converged simulation results. This method of applying ΔP has been thoroughly described in a previous study [40] and adopted by many other researchers to simulate the membrane process [41–44]. To enhance the signal-to-noise ratio and accelerate the NEMD simulations, like other simulating studies [41–46] we perform the simulations under very high ΔPs (100 MPa-600 MPa), which are much higher than pressures applied in experiments and industrial usage.

Conflicts of Interest

The authors declare that there are no conflicts of interest.

Authors' Contributions

Yong Wang supervised this research. Fang Xu and Mingjie Wei conducted the simulations with assistance from Xin Zhang, Zhou Wei and Yang Song. All authors discussed and analyzed results. Fang Xu, Mingjie Wei, and Yong Wang wrote the manuscript with inputs from other authors. Fang Xu and Mingjie Wei contributed equally to this work.

Acknowledgments

Financial supports from the National Basic Research Program of China (2015CB655301), the National Key Research and Development Program of China (2017YFC0403902), the National Natural Science Foundation of China (21825803; 21506091), and the Jiangsu Natural Science Foundations (BK20150944; BK20150063) are acknowledged. We are grateful to the High Performance Computing Center of Nanjing Tech University and the National Supercomputing Center in Wuxi (Sunway Taihu Light) for supporting the computational resources. We also thank the Program of Excellent Innovation Teams of Jiangsu Higher Education Institutions and the Project of Priority Academic Program Development of Jiangsu Higher Education Institutions (PAPD) for supports.

Supplementary Materials

Calculation of water flux by fitting the slope of the flow curve. The numbers of water molecules in the feed side, inside the pores, and in the permeate side were tracked over simulation time. To justify the steady state of the system, Figure S1 shows an exemplificative evolution of numbers of water molecules in the three phases over the sampling period for the membrane with a 0.8 nm-wide pore and a contact angle of 29°. In Figure S1, the blue region represents the numbers of water molecules in feed side, while the grass green region represents those in permeate side. The number of water molecules in feed side drops linearly as a function of simulation time; at the same time, the number for permeate side rises linearly. The dark green region represents the number of water molecules in the inner part. The height of this part is unchanged, indicating the constant number of water molecules in the inner part. Besides, the linear relationship indicates that water molecules permeate through the membrane at a constant rate. Therefore, the slope of the flow curve in Figure S1 corresponds to the water flux. *(Supplementary Materials)*

References

[1] J. R. Werber, C. O. Osuji, and M. Elimelech, "Materials for next-generation desalination and water purification membranes," *Nature Reviews Materials*, vol. 1, Article ID 16018, 2016.

[2] Q. Xu, Y. Yang, X. Wang et al., "Atomic layer deposition of alumina on porous polytetrafluoroethylene membranes for enhanced hydrophilicity and separation performances," *Journal of Membrane Science*, vol. 415-416, pp. 435–443, 2012.

[3] F. Yan, H. Chen, Y. Lü et al., "Improving the water permeability and antifouling property of thin-film composite polyamide nanofiltration membrane by modifying the active layer with triethanolamine," *Journal of Membrane Science*, vol. 513, pp. 108–116, 2016.

[4] Y. Zhao, Z. Zhang, L. Dai, H. Mao, and S. Zhang, "Enhanced both water flux and salt rejection of reverse osmosis membrane through combining isophthaloyl dichloride with biphenyl tetraacyl chloride as organic phase monomer for seawater desalination," *Journal of Membrane Science*, vol. 522, pp. 175–182, 2017.

[5] J. Goldsmith and C. C. Martens, "Molecular dynamics simulation of salt rejection in model surface-modified nanopores," *The Journal of Physical Chemistry Letters*, vol. 1, no. 2, pp. 528–535, 2010.

[6] S. Joseph and N. R. Aluru, "Why are carbon nanotubes fast transporters of water?" *Nano Letters*, vol. 8, no. 2, pp. 452–458, 2008.

[7] L. Wang, R. S. Dumont, and J. M. Dickson, "Nonequilibrium molecular dynamics simulation of pressure-driven water transport through modified CNT membranes," *The Journal of Chemical Physics*, vol. 138, no. 12, Article ID 124701, 2013.

[8] T.-D. Li, J. Gao, R. Szoszkiewicz, U. Landman, and E. Riedo, "Structured and viscous water in subnanometer gaps," *Physical Review B: Condensed Matter and Materials Physics*, vol. 75, no. 11, 2007.

[9] T. Wei, L. Zhang, H. Zhao et al., "Aromatic polyamide reverse-osmosis membrane: an atomistic molecular dynamics simulation," *The Journal of Physical Chemistry B*, vol. 120, no. 39, pp. 10311–10318, 2016.

[10] M. E. Suk and N. R. Aluru, "Water transport through ultrathin graphene," *The Journal of Physical Chemistry Letters*, vol. 1, no. 10, pp. 1590–1594, 2010.

[11] F. Xu, Y. Song, M. Wei, and Y. Wang, "Water flow through interlayer channels of two-dimensional materials with various hydrophilicities," *The Journal of Physical Chemistry C*, vol. 122, no. 27, pp. 15772–15779, 2018.

[12] R. R. Nair, H. A. Wu, P. N. Jayaram, I. V. Grigorieva, and A. K. Geim, "Unimpeded permeation of water through helium-leak-tight graphene-based membranes," *Science*, vol. 335, pp. 442–444, 2012.

[13] W.-G. Kim and S. Nair, "Membranes from nanoporous 1D and 2D materials: A review of opportunities, developments, and challenges," *Chemical Engineering Science*, vol. 104, pp. 908–924, 2013.

[14] W. Hirunpinyopas, E. Prestat, S. D. Worrall, S. J. Haigh, R. A. W. Dryfe, and M. A. Bissett, "Desalination and nanofiltration through functionalized laminar MoS2 membranes," *ACS Nano*, vol. 11, no. 11, pp. 11082–11090, 2017.

[15] G. Liu, W. Jin, and N. Xu, "Two-dimensional-material membranes: a new family of high-performance separation membranes," *Angewandte Chemie International Edition*, vol. 55, no. 43, pp. 13384–13397, 2016.

[16] L. Sun, Y. Ying, H. Huang et al., "Ultrafast molecule separation through layered WS2 nanosheet membranes," *ACS Nano*, vol. 8, no. 6, pp. 6304–6311, 2014.

[17] L. Sun, H. Huang, and X. Peng, "Laminar MoS2 membranes for molecule separation," *Chemical Communications*, vol. 49, no. 91, pp. 10718–10720, 2013.

[18] C. E. Ren, K. B. Hatzell, M. Alhabeb, Z. Ling, K. A. Mahmoud, and Y. Gogotsi, "Charge- and size-selective ion sieving through Ti3C2Tx mxene membranes," *The Journal of Physical Chemistry Letters*, vol. 6, no. 20, pp. 4026–4031, 2015.

[19] N. Wei, X. Peng, and Z. Xu, "Breakdown of fast water transport in graphene oxides," *Physical Review E: Statistical, Nonlinear, and Soft Matter Physics*, vol. 89, no. 1, Article ID 012113, 2014.

[20] B. Chen, H. Jiang, X. Liu, and X. Hu, "Observation and analysis of water transport through graphene oxide interlamination," *The Journal of Physical Chemistry C*, vol. 121, no. 2, pp. 1321–1328, 2017.

[21] B. Liu, R. Wu, J. A. Baimova et al., "Molecular dynamics study of pressure-driven water transport through graphene bilayers," *Physical Chemistry Chemical Physics*, vol. 18, no. 3, pp. 1886–1896, 2016.

[22] J. Muscatello, F. Jaeger, O. K. Matar, and E. A. Müller, "Optimizing water transport through graphene-based membranes: insights from nonequilibrium molecular dynamics," *ACS Applied Materials & Interfaces*, vol. 8, no. 19, pp. 12330–12336, 2016.

[23] R. H. Tunuguntla, R. Y. Henley, Y.-C. Yao, T. A. Pham, M. Wanunu, and A. Noy, "Enhanced water permeability and tunable ion selectivity in subnanometer carbon nanotube porins," *Science*, vol. 357, no. 6353, pp. 792–796, 2017.

[24] K. Huang, G. Liu, J. Shen et al., "High-efficiency water-transport channels using the synergistic effect of a hydrophilic polymer and graphene oxide laminates," *Advanced Functional Materials*, vol. 25, no. 36, pp. 5809–5815, 2015.

[25] N. Wei, X. Peng, and Z. Xu, "Understanding water permeation in graphene oxide membranes," *ACS Applied Materials & Interfaces*, vol. 6, no. 8, pp. 5877–5883, 2014.

[26] D. A. Dikin, S. Stankovich, E. J. Zimney et al., "Preparation and characterization of graphene oxide paper," *Nature*, vol. 448, no. 7152, pp. 457–460, 2007.

[27] N. R. Wilson, P. A. Pandey, R. Beanland et al., "Graphene oxide: structural analysis and application as a highly transparent support for electron microscopy," *ACS Nano*, vol. 3, no. 9, pp. 2547–2556, 2009.

[28] P. V. Kumar, N. M. Bardhan, S. Tongay, J. Wu, A. M. Belcher, and J. C. Grossman, "Scalable enhancement of graphene oxide properties by thermally driven phase transformation," *Nature Chemistry*, vol. 6, no. 2, pp. 151–158, 2014.

[29] K. Erickson, R. Erni, Z. Lee, N. Alem, W. Gannett, and A. Zettl, "Determination of the local chemical structure of graphene oxide and reduced graphene oxide," *Advanced Materials*, vol. 22, no. 40, pp. 4467–4472, 2010.

[30] S. Ban, J. Xie, Y. Wang, B. Jing, B. Liu, and H. Zhou, "Insight into the nanoscale mechanism of rapid H2O transport within a graphene oxide membrane: impact of oxygen functional group clustering," *ACS Applied Materials & Interfaces*, vol. 8, no. 1, pp. 321–332, 2016.

[31] S. Zheng, Q. Tu, J. J. Urban, S. Li, and B. Mi, "Swelling of graphene oxide membranes in aqueous solution: characterization of interlayer spacing and insight into water transport mechanisms," *ACS Nano*, vol. 11, no. 6, pp. 6440–6450, 2017.

[32] M. Hu and B. Mi, "Layer-by-layer assembly of graphene oxide membranes via electrostatic interaction," *Journal of Membrane Science*, vol. 469, pp. 80–87, 2014.

[33] W. L. Jorgensen, D. S. Maxwell, and J. Tirado-Rives, "Development and testing of the OPLS all-atom force field on conformational energetics and properties of organic liquids," *Journal of the American Chemical Society*, vol. 118, no. 45, pp. 11225–11236, 1996.

[34] B. Chen, H. Jiang, X. Liu, and X. Hu, "Molecular insight into water desalination across multilayer graphene oxide membranes," *ACS Applied Materials & Interfaces*, vol. 9, no. 27, pp. 22826–22836, 2017.

[35] Z. Zheng, C. T. Nottbohm, A. Turchanin et al., "Janus nanomembranes: A generic platform for chemistry in two dimensions," *Angewandte Chemie International Edition*, vol. 49, no. 45, pp. 8493–8497, 2010.

[36] L. Zhang, J. Yu, M. Yang, Q. Xie, H. Peng, and Z. Liu, "Janus graphene from asymmetric two-dimensional chemistry," *Nature Communications*, vol. 4, no. 1, Article ID 1443, 2013.

[37] J. Abraham, K. S. Vasu, C. D. Williams et al., "Tunable sieving of ions using graphene oxide membranes," *Nature Nanotechnology*, vol. 12, no. 6, pp. 546–550, 2017.

[38] T. Werder, J. H. Walther, R. L. Jaffe, T. Halicioglu, and P. Koumoutsakos, "On the water-carbon interaction for use in molecular dynamics simulations of graphite and carbon nanotubes," *The Journal of Physical Chemistry B*, vol. 107, no. 6, pp. 1345–1352, 2003.

[39] S. E. Strong and J. D. Eaves, "The dynamics of water in porous two-dimensional crystals," *The Journal of Physical Chemistry B*, vol. 121, no. 1, pp. 189–207, 2016.

[40] C. Huang, K. Nandakumar, P. Y. K. Choi, and L. W. Kostiuk, "Molecular dynamics simulation of a pressure-driven liquid transport process in a cylindrical nanopore using two self-adjusting plates," *The Journal of Chemical Physics*, vol. 124, no. 23, Article ID 234701, 2006.

[41] D. Cohen-Tanugi, L.-C. Lin, and J. C. Grossman, "Multilayer nanoporous graphene membranes for water desalination," *Nano Letters*, vol. 16, no. 2, pp. 1027–1033, 2016.

[42] D. Cohen-Tanugi and J. C. Grossman, "Water desalination across nanoporous graphene," *Nano Letters*, vol. 12, no. 7, pp. 3602–3608, 2012.

[43] M. Heiranian, A. B. Farimani, and N. R. Aluru, "Water desalination with a single-layer MoS 2 nanopore," *Nature Communications*, vol. 6, Article ID 8616, 2015.

[44] M. Shen, S. Keten, and R. M. Lueptow, "Dynamics of water and solute transport in polymeric reverse osmosis membranes via molecular dynamics simulations," *Journal of Membrane Science*, vol. 506, pp. 95–108, 2016.

[45] M. Ding, A. Szymczyk, F. Goujon, A. Soldera, and A. Ghoufi, "Structure and dynamics of water confined in a polyamide reverse-osmosis membrane: A molecular-simulation study," *Journal of Membrane Science*, vol. 458, pp. 236–244, 2014.

[46] W. Gao, F. She, J. Zhang et al., "Understanding water and ion transport behaviour and permeability through poly(amide) thin film composite membrane," *Journal of Membrane Science*, vol. 487, pp. 32–39, 2015.